DOI 10.1007/s11106-019-00051-6
Powder Metallurgy and Metal Ceramics, Vol. 58, Nos. 1-2, May, 2019 (Russian Original Vol. 58, Nos. 1-2, Jan.-Feb., 2019)

PHASE EQUILIBRIA IN THE La_2O_3–Er_2O_3 SYSTEM IN THE TEMPERATURE RANGE 1100–1500°C

O.A. Kornienko,[1,2] O.V. Chudinovych,[1] A.I. Bykov,[1] A.V. Samelyuk,[1] and E.R. Andrievskaya[1*]

UDC 621.762; 541.123.3

Phase equilibria and structural transformations in the binary La_2O_3–Er_2O_3 system at 1100–1500°C have been studied by X-ray diffraction, microstructural analysis, and electron microprobe analysis over the entire composition range. Solid solutions based on the hexagonal modification of A-La_2O_3, cubic modification of C-Er_2O_3, and ordered perovskite-type $LaErO_3$ (R) phase with orthorhombic distortion have been established to exist in the system. The boundaries of phase regions and lattice parameters of the phases formed in the system have been determined. The ordered perovskite-type $LaErO_3$ (R) phase is present in the composition range 45–51 mol.% Er_2O_3 at 1100 and 1500°C. When temperature decreases to 1100°C, the homogeneity ranges of the C-Er_2O_3 and A-La_2O_3 solid solutions are reduced. The complete La_2O_3–Er_2O_3 phase diagram has been constructed over the composition range 800–2400°C using literature data.

Keywords: *lanthanum and erbium oxides, phase equilibria, solid solutions, functional and structural ceramics.*

INTRODUCTION. LITERATURE REVIEW. PROBLEM STATEMENT

The development and evolution of technology increasingly call for new materials. Rare earth metal (REM) oxides are promising for the development of materials for wide applications: electronic engineering, optoelectronics, nuclear and laser technology, medicine, etc. [1–3]. This in turn necessitates the study of phase equilibria in multicomponent REM oxide systems. Of scientific interest is to examine the polymorphic features, the formation or decomposition of solid solutions and ordered phases, and the effect of electronic structure and ionic radii of lanthanides on the phase transformations, structure, and stability of phases in the REM oxide systems.

Materials consisting of phases with ABO_3 perovskite structure are extensively used in various fields of technology. Many characteristics of these materials (such as electronic or ionic conductivity, dielectric constant, and magnetic moment) are sensitive to any changes in the structure of ABO_3 phases [4]. Particular physicochemical properties are acquired by either an ideal structure without defects or a structure with defects resulting from the substitution of cations in positions A and B [5].

*Deceased.

[1]Frantsevich Institute for Problems of Materials Science, National Academy of Sciences of Ukraine, Kyiv, Ukraine.

[2]To whom correspondence should be addressed; e-mail: kornienkooksana@ukr.net.

Translated from Poroshkova Metallurgiya, Vol. 58, Nos. 1–2 (525), pp. 113–123, 2019. Original article submitted June 22, 2018.

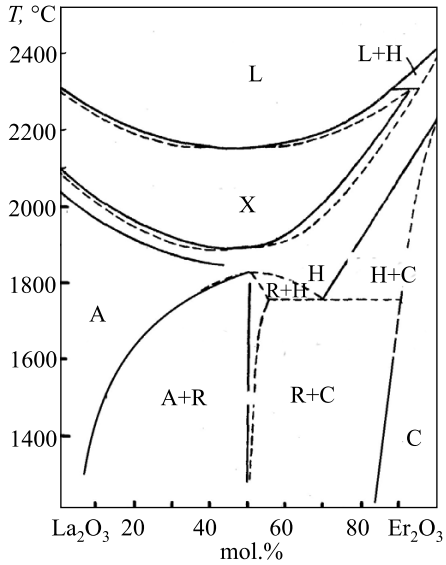

Fig. 1. The La_2O_3–Er_2O_3 phase diagram [10]

Especially interesting heterovalent substitution in the ABO_3 structure occurs when the lattice charge is compensated through a large number of oxygen vacancies. This leads to a structure with mixed electronic and ionic conductivity [6].

The perovskite structure in the binary La_2O_3–Ln_2O_3 system originates with holmium oxide since Goldschmidt tolerance factor t is 0.786, 0.790, 0.793, 0.798, and 0.800 for $LaHoO_3$, $LaErO_3$, $LaTmO_3$, $LaYbO_3$, and $LaLuO_3$, respectively [7].

The phase relations and structures of the phases formed in the La_2O_3–Er_2O_3 system are examined in [8–13]. It should be noted that this system was studied both experimentally [10] and by thermodynamic calculations [13]. The data obtained are graphically interpreted in Figs. 1 and 2.

According to X-ray diffraction, an ordered $LaErO_3$ (R) perovskite-type phase with a narrow homogeneity range forms in the La_2O_3–Er_2O_3 system [11]. The lattice parameters of the ordered stoichiometric $LaErO_3$ phase are as follows: a = 0.5864 nm, b = 0.6082 nm, and c = 0.8466 nm. The compound remains stable up to 1800°C and then transfers to a hexagonal (H) La_2O_3 solid solution [10]. In the above system, there are solid solutions of cubic (C) and hexagonal (H) Er_2O_3 modifications and low-temperature hexagonal (A) and high-temperature hexagonal (H) and cubic (X) Ln_2O_3 modifications. The paper [14] establishes temperatures of La_2O_3 phase transformations: A ⇄ ⇄ H at 2050°C and H ⇄ X at 2140°C, T_{melt} = 2310°C. Polymorphic transformations C ⇄ B, B ⇄ A, and A ⇄ H for Er_2O_3 proceed in a narrow temperature range (~2320°C); hence, the phase diagram shows only phase transformation C ⇄ H at T = 2390°C.

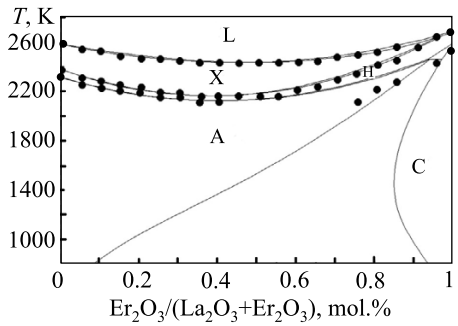

Fig. 2. The Er_2O_3–La_2O_3 phase diagram according to the thermodynamic calculation [13]

Phase transition A ⇄ H in the La_2O_3–Er_2O_3 system was established by thermal analysis in the composition range with high La_2O_3 content, but the boundaries of phase fields were not determined [10]. The liquidus surface of the La_2O_3–Er_2O_3 system is characterized by a minimum near the 45 mol.% Er_2O_3 field and by peritectic transformation L + H ⇄ X.

Unlike previous data, the paper [13] found no R perovskite phase (Fig. 2). It should be noted that the phase diagram of the above system in [13] is based on thermodynamic calculations. The data indicate that only solid solutions of hexagonal A-La_2O_3 and cubic C-Er_2O_3 modifications that are separated by a two-phase (A + C) region form in the La_2O_3–Er_2O_3 system. The two-phase region substantially expands with decreasing temperature.

Hence, the literature shows that data on the phase equilibria in the binary La_2O_3–Er_2O_3 system concerning the ordered $LaErO_3$ perovskite-type phase and boundaries of solid solutions are contradictory and do not agree (in some cases, the Gibbs phase rule does not hold in this phase diagram, etc.) Therefore, the phase equilibria in this system are to be clarified.

The objective of the paper is to construct the La_2O_3–Er_2O_3 phase diagram in the range 800–2400°C.

EXPERIMENTAL PROCEDURE

The starting materials were La_2O_3 of LaO-1 grade and Er_2O_3 of Ero-2 grade (content of the main components reaches 99.99%). Before being weighed, the oxides were dried in a muffle chamber at 1200°C (2 h). The charges were prepared with a concentration step of 1–5 mol.%. Weighed oxide portions were dissolved in HNO_3 (1 : 1), evaporated, and calcined at 800°C for 2 h. The powders were subjected to single-action pressing in a steel die without a binder at 10–30 MPa to make pellets 5 mm in diameter and 4 mm in height. Two-stage heat-treatment regime was chosen to homogenize the charges: (i) calcination in a furnace with H23U5T heaters (iron–aluminum heat-resistant alloy) at 1100°C for 744 h (to remove residual nitrates) and (ii) annealing in a furnace with heaters made of molybdenum disilicide $MoSi_2$ at 1500°C for 225 h in air (to induce diffusion-controlled composition homogenization in accordance with the phase diagram). The samples were cooled down with the

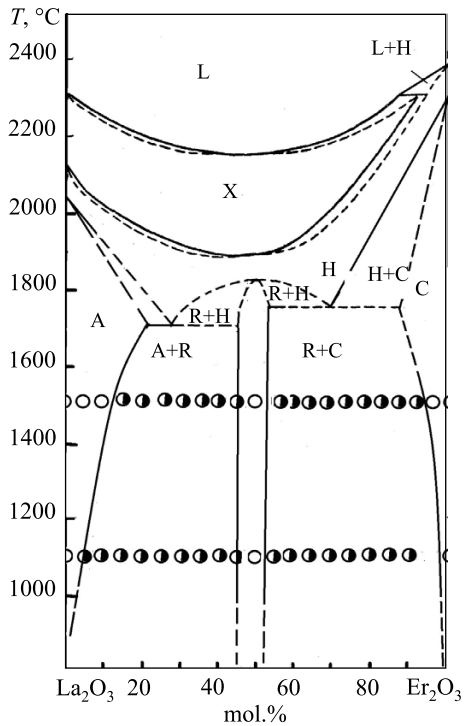

Fig. 3. The La_2O_3–Er_2O_3 phase diagram (according to [10] above 1500°C); *1*) single-phase and *2*) two-phase regions (according to our studies)

TABLE 1. Phase Composition and Lattice Parameters of Samples in the

Chemical composition, mol.%		Phase composition at T = 1500°C	Lattice parameters of the phases, nm ($a \pm 0.0002$), T = 1500°C					
			<A>*		<C>	R		
La_2O_3	Er_2O_3		*a*	*c*	*a*	*a*	*b*	*c*
100	0	<A>*	0.6529	0.3857	–			
95	5	< A>*	0.6504	0.3828	–	–	–	–
90	10	< A>*	0.6483	0.3849	–	–	–	–
85	15	<A>*+ R_{traces}	0.6477	0.3815	–	–	–	–
80	20	<A>* + R↑	0.6468	0.3787	–	0.6056	0.5852	0.8428
75	25	<A>*↓ + R↑	0.6466	0.3819	–	0.6065	0.5861	0.8458
70	30	<A>*↓ + R↑	0.6464	0.3794	–	0.6086	0.5855	0.8447
65	35	<A>*↓ + R↑	0.6494	0.3821	–	0.6087	0.5853	0.8483
60	40	<A>*↓ + R↑	0.6470	0.3806	–	0.6058	0.5846	0.8447
55	45	<A>*↓ + R↑	0.6450	0.3829	–	0.6068	0.5862	0.8442
50	50	R	–	–	–	0.6056	0.5843	0.8442
49	51	R	–	–	–	0.6060	0.5856	0.8416
48	52	R + $<C>_{traces}$	–	–	–	0.6048	0.5854	0.8437
47	53	R + <C>↑	–	–	–	0.6064	0.5851	0.8435
46	54	R + < C>↑	–	–	–	0.6056	0.5843	0.8442
45	55	R + <C>↑	–	–	1.0589	0.6048	0.5849	0.8440
40	60	R + <C>↑	–	–	1.0602	0.6048	0.5860	0.8435
35	65	R↓ + <C>	–	–	1.0606	0.6081	0.5852	0.8426
30	70	R↓ + <C>	–	–	1.0609	0.6121	0.5839	0.8411
25	75	R↓ + <C>	–	–	1.0601	0.6052	0.5848	0.8426
20	80	R↓ + <C>	–	–	1.0606	0.6125	0.5794	0.8433
15	85	R↓ + <C>	–	–	1.0610	0.6125	0.5858	0.8393
10	90	R↓ + <C>	–	–	1.0602	–	–	–
5	95	<C>	–	–	1.0572	–	–	–
0	100	<C>	–	–	1.0531	–	–	–

Notes. The * sign denotes the hexagonal A-La_2O_3 modification that becomes hydrated in specific annealing conditions phases are denoted as <A> for solid solutions based on the hexagonal La_2O_3 modification, <C> for solid solutions based or decreases (↓).

furnace. In the low-temperature range (≤1250°C), the phase equilibria including the decomposition and ordering processes are established rather slowly because of low speed of diffusion processes in the cation sublattice, which requires long-term annealing of the samples [15]. To check whether the synthesis was complete in specific time intervals, the samples were ground and pressed and subjected to further heat treatment. No change in the samples' phase composition was observed after annealing for 225 and 9820 h at 1500 and 1100°C.

A DRON-3 diffractometer was employed for X-ray powder diffraction (XRD) of the samples at room temperature (Cu-K_α radiation, Ni filter). The scanning angle was 0.05–0.1° and exposure time was 4 sec in the range 2θ = 10–100°. The lattice parameters were calculated using the least-squares method with the LATTICE software (with an error not lower than 0.0002 nm for the cubic phase).

To establish the phase composition, the database of the International Center for Diffraction Data was used (JSPSDS International Center for Diffraction Data 1999).

La_2O_3–Er_2O_3 System Annealed at 1500°C (225 h) and 1100°C (9820 h)

Phase composition at T = 1100°C	Lattice parameters of the phases, nm (a ± 0.0002), T = 1100°C					
	<A>*		<C>	R		
	a	c	a	a	b	c
<A>*	0.6529	0.3857	–	–	–	–
<A>*+ R_{traces}	0.6504	0.3828	–	–	–	–
< A>* + R↑	0.6503	0.3823	–	0.6061	0.5845	0.8452
< A>* + R↑	0.6514	0.3833	–	0.6056	0.5872	0.8461
<A>* + R↑	0.6491	0.3825	–	0.6048	0.5851	0.8431
<A>*↓ + R↑	0.6494	0.3825	–	0.6065	0.5835	0.8467
<A>*↓ + R↑	0.6504	0.3823	–	0.6046	0.5853	0.8453
<A>*↓ + R↑	0.6517	0.3821	–	0.6063	0.5859	0.8453
<A>*↓+ R↑	0.6501	0.3821	–	0.6063	0.5852	0.8459
<A>*↓+ R↑	0.6514	0.3822	–	0.6071	0.5855	0.8454
R	–	–	–	0.6059	0.5854	0.8447
R + <C>	–	–	–	0.6064	0.5859	0.8453
R + $<C>_{traces}$	–	–	–	0.6052	0.5844	0.8443
R + <C>↑	–	–	–	0.6063	0.5851	0.8453
R + <C>↑	–	–	1.0539	0.6060	0.5846	0.8446
R + <C>↑	–	–	1.0570	0.6064	0.5861	0.8467
R + <C>↑	–	–	1.0587	0.6062	0.5859	0.8466
R + <C>↑	–	–	1.0542	0.6056	0.5850	0.8432
R↓ + <C>	–	–	1.0568	0.6058	0.5828	0.8443
R↓ +<C>	–	–	1.0574	0.6058	0.5853	0.8459
R↓ + <C>	–	–	1.0564	0.6041	0.5851	0.8485
R↓ + <C>	–	–	1.0568	0.6047	0.5879	0.8433
R_{traces} + <C>	–	–	1.0569	–	–	–
–	–	–	–	–	–	–
<C>	–	–	1.0531	–	–	–

(T = 1500°C (225 h) and T = 1100°C (9820 h) in air) to form the hexagonal modification of A-$La(OH)_3$ hydroxide. The on the cubic Er_2O_3 modification, and R for the ordered $LaErO_3$ phase of perovskite type. The phase content increases (↑)

The microstructure was examined on unetched sections of annealed samples coated with a gold layer using a Superprobe-733 scanning electron microscope (JEOL, Japan; Palo Alto, CA) in backscattered electrons (BSE).

If content of the second phase was too low to be determined by XRD, the phase composition of the samples was refined by polarization microscopy. Petrographic studies were conducted on annealed samples in polarized transmission light. The crystal optic characteristics of the phases were determined using a MIN-8 polarized microscope. The refractive indices were measured in immersion liquids with high refractive indices (arsenic tribromide solution in methylene iodide and alloys of sulfur with selenium) with an error of ±0.02.

DISCUSSION OF RESULTS

The solid-phase interaction of La_2O_3 (hexagonal A modification) and Er_2O_3 (cubic C modification of REM oxides, Tl_2O_3-type structure) was studied in the range 1100–1500°C. Three types of solid solutions formed in the

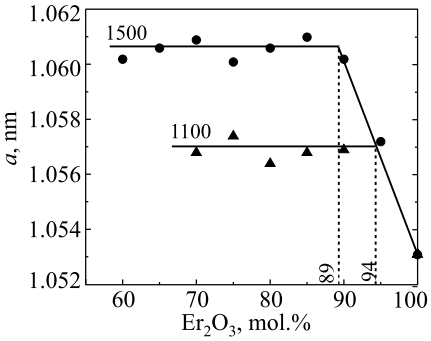

Fig. 4

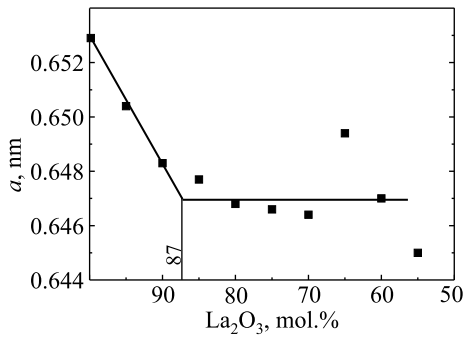

Fig. 5

Fig. 4. Composition dependences of the lattice parameters of C-Er_2O_3 solid solutions in the La_2O_3–Er_2O_3 system after annealing at 1100 and 1500°C

Fig. 5. Composition dependence of the lattice parameters of the A*-La_2O_3 solid solutions in the La_2O_3–Er_2O_3 system after annealing at 1500°C

La_2O_3–Er_2O_3 system: solutions based on (i) hexagonal A-La_2O_3 modification, (ii) cubic C-Er_2O_3 modification, and (iii) ordered $LaErO_3$ (R) phase crystallized in the perovskite-type structure with orthorhombic distortion. These solutions are separated by two-phase A + R and R + C fields (Fig. 3).

The starting chemical and phase compositions of the samples annealed at 1500 and 1100°C and the lattice parameters of phases in equilibria at these temperatures are provided in Table 1.

The composition dependences of the lattice parameters of the C-Er_2O_3 and A-La_2O_3 solid solutions at 1100 and 1500°C are shown in Figs. 4 and 5, respectively. According to XRD, the homogeneity ranges of the A-

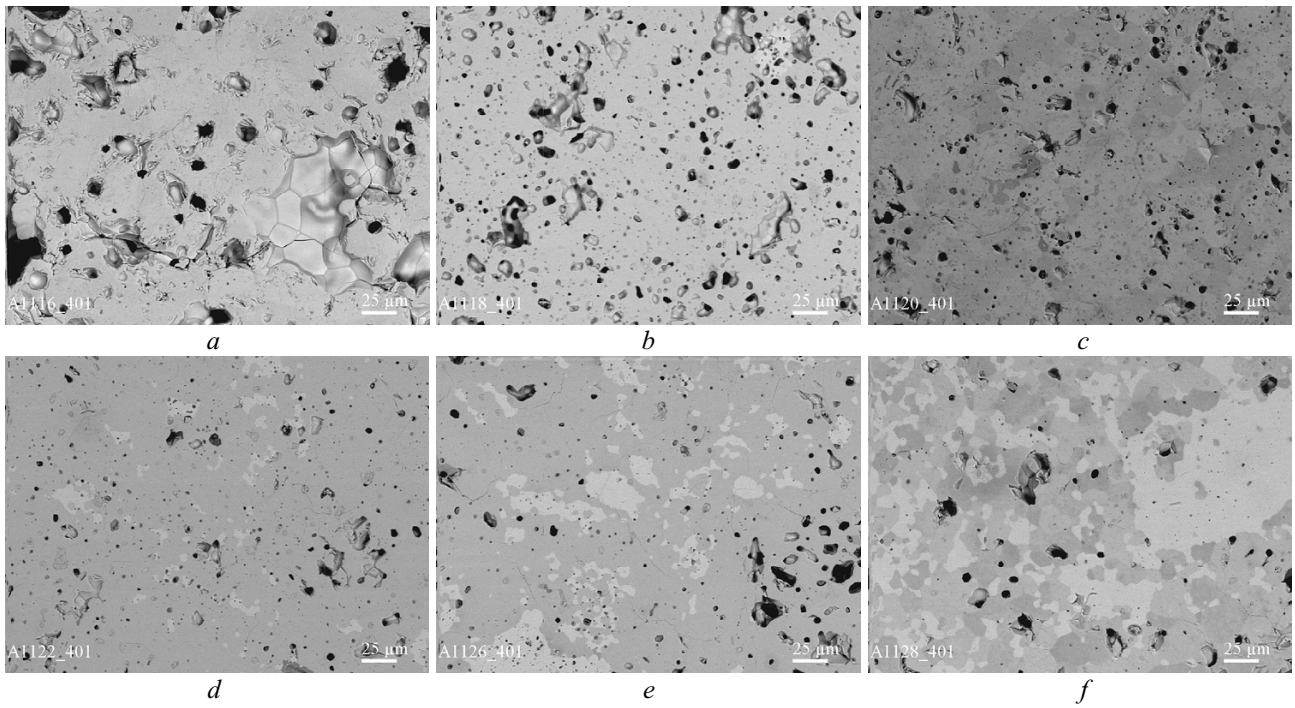

Fig. 6. Microstructures of the La_2O_3–Er_2O_3 samples annealed at 1500°C: *a*) 50 mol.% La_2O_3–50 mol.% Er_2O_3 (<R>); *b*) 49 mol.% La_2O_3–51 mol.% Er_2O_3 (<R>+<C-Er_2O_3>); *c*) 48 mol.% La_2O_3–52 mol.% Er_2O_3 (<R>+<C-Er_2O_3>); *d*) 40 mol.% La_2O_3–60 mol.% Er_2O_3 (<R>+<C-Er_2O_3>); *e*) 15 mol.% La_2O_3–85 mol.% Er_2O_3 (<R>+<C-Er_2O_3>); *f*) 10 mol.% La_2O_3–90 mol.% Er_2O_3 (<R>+ +<C-Er_2O_3>); anisotropic R phase is dark, isotropic C-Er_2O_3 phase is light, pores are black areas

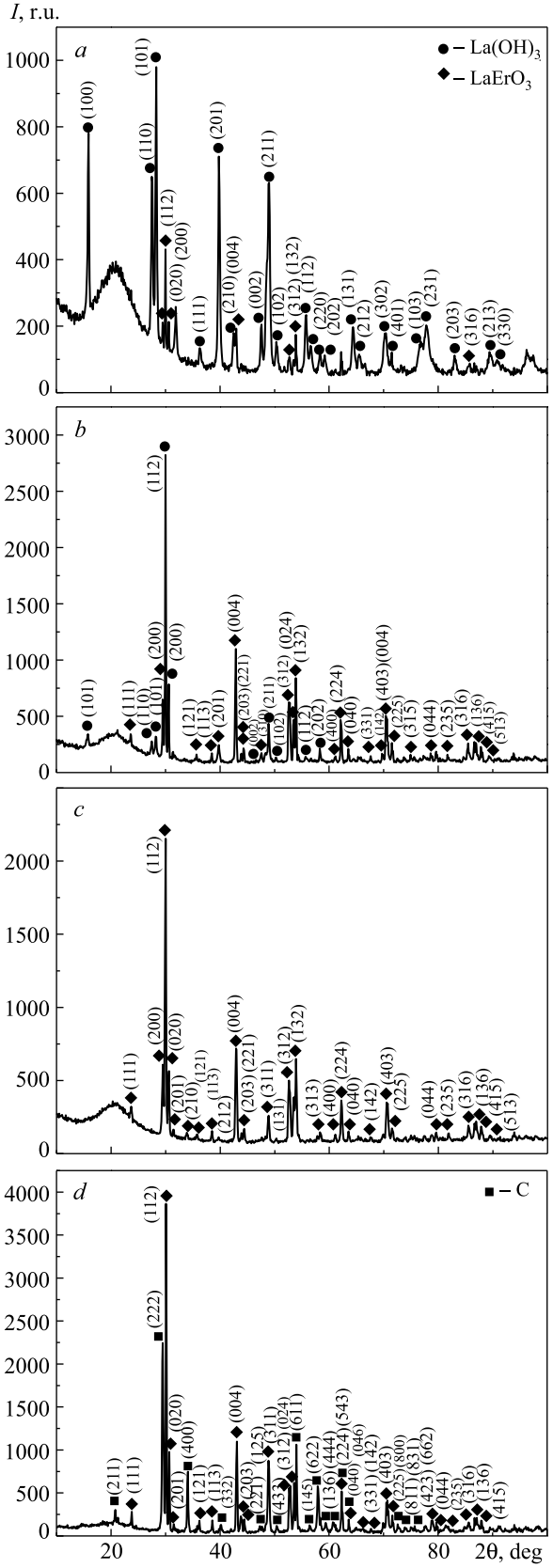

Fig. 7. X-ray diffraction patterns of the La_2O_3–Er_2O_3 samples annealed at 1100°C: *a*) 90% La_2O_3–10% Er_2O_3 (A*+$LaErO_3$ (R)); *b*) 55% La_2O_3–45% Er_2O_3 (A*+$LaErO_3$ (R)); *c*) 50% La_2O_3–50% Er_2O_3 ($LaErO_3$ (R)); *d*) 35% La_2O_3–65% Er_2O_3 ($LaErO_3$ (R) + C)

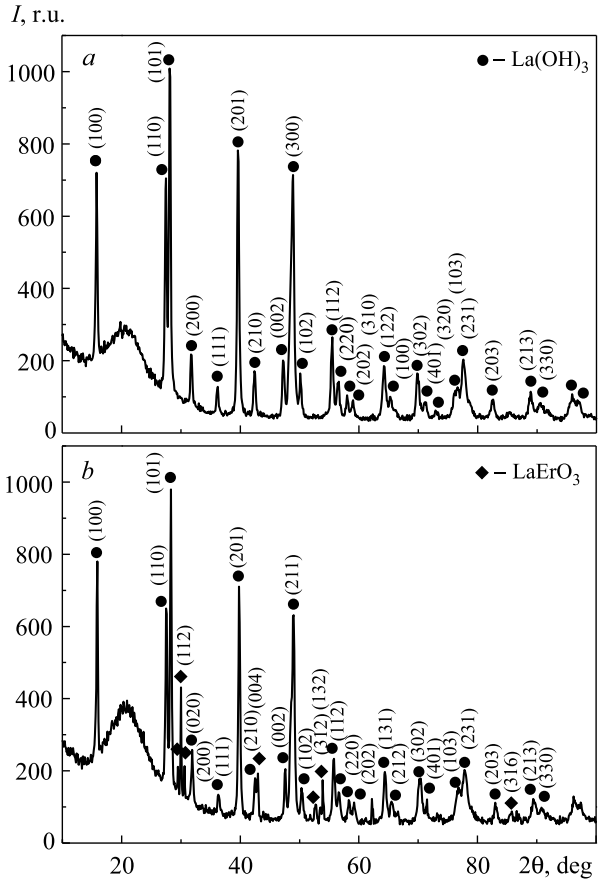

Fig. 8. Diffraction patterns of the La_2O_3–Er_2O_3 samples annealed at 1500°C: *a*) 90 mol.% La_2O_3–10 mol.% Er_2O_3 (A*); *b*) 85 mol.% La_2O_3–15 mol.% Er_2O_3 (A*+$LaErO_3$ (R))

La_2O_3, C-Er_2O_3, and R-phase ($LaErO_3$) solid solutions determine the compositions that contain 10–15, 90–95 and 45–50, and 50–51 mol.% Er_2O_3 at 1500°C and 0–5, 90–100 and 45–50, and 50–51 mol.% Er_2O_3 at 1100°C (Fig. 4). The data show that the solubility of La_2O_3 in the cubic C-Er_2O_3 modification is ~11 mol.% at 1500°C and ~6 mol.% at 1100°C (Fig. 4). The lattice parameters increase from a = 1.0531 nm for pure Er_2O_3 to a = 1.0602 nm (at 1500°C) and a = 1.0569 nm (at 1100°C) for the two-phase sample containing 10 mol.% La_2O_3.

The solubility of Er_2O_3 in the hexagonal A-La_2O_3 modification is ~5 mol.% at 1100°C and ~13 mol.% at 1500°C (Fig. 5). It should be noted that the samples with a higher lanthanum oxide content after annealing and cooling rapidly absorb water in humid air and become hydrated. Hence, according to XRD, the hexagonal A-$La(OH)_3$ modification forms instead of the hexagonal A-La_2O_3 phase in the samples containing from 55 to 100 mol.% La_2O_3. The lattice parameters of this phase change from a = 0.6529 nm and c = 0.3857 nm in pure $La(OH)_3$ to a = 0.6477 nm and c = 0.3815 nm in the two-phase (A + R) sample containing 15 mol.% Er_2O_3 (at 1500°C) and to a = 0.6504 nm and c = 0.3828 nm in the A + R sample containing 5 mol.% Er_2O_3 (at 1100°C). In the composition range 90–100 mol.% La_2O_3 (at 1500°C), there is only one phase that belongs to the hexagonal $La(OH)_3$ modification. According to petrographic data, the anisotropic A-$La(OH)_3$ phase is manifested as lamellar crystals of gray and yellow interference tints.

According to [11], the stoichiometric perovskite-type phase has the following lattice parameters: a = = 0.5864 nm, b = 0.6082 nm, and c = 0.8466 nm. The experimental values have small deviations, which may indicate that additional vacancies form in the $LaErO_3$ lattice in the conditions in question.

Crystal optic analysis confirmed the XRD data for the two-phase (C + R) sample containing 5 mol.% La_2O_3–95 mol.% Er_2O_3 (at 1100°C). Two structural components are clearly seen: semitransparent isotropic C-Er_2O_3 phase (base) and anisotropic $LaErO_3$ phase with bright interference tints, present in a smaller amount. In the composition range 10–48 mol.% Er_2O_3, the samples contain the anisotropic R phase along with the isotropic C-Er_2O_3 phase, and the content of the anisotropic $LaErO_3$ phase noticeably increases with higher erbium oxide content. The sample containing 95 mol.% Er_2O_3 has only one isotropic phase, C-Er_2O_3.

According to XRD and microstructural analysis, the ordered $LaErO_3$ (R) phase exists in the composition range 45–51 mol.% Er_2O_3 at 1500 and 1100°C.

The microstructure of the ordered stoichiometric $LaErO_3$ phase is shown in Fig. 6*a* and the microstructures that correspond to the two-phase C + R region in the phase diagram are shown in Fig. 6*b–f*. The samples containing from 10 to 49 mol.% La_2O_3 have two clear structural components: gray anisotropic porous R phase and light isotropic C phase. It should be noted that X-ray diffraction of the sample with 90 mol.% Er_2O_3 did not reveal the ordered perovskite-type phase, while the microstructure of the sample clearly shows that this phase is present in a small amount. The presence of two phases was confirmed by crystal optic studies. Thus, there is less than 5 mol.% of the perovskite-type phase in the sample.

The ordering of the $LaErO_3$ phase is a gradual diffusion-controlled process. In the early sintering stage, the samples acquire high relative density, and then the R phase becomes ordered in the dense ceramics. This leads to a great number of pores concentrated at grain boundaries of the C-Er_2O_3 light phase and dark gray grains of the ordered R phase. The C-Er_2O_3 phase contains almost zero pores, while the R phase has a great number of pores. The substitution of Er^{3+} ions by La^{3+} ions is accompanied by a phase transition ($C \rightarrow R$) with simultaneous shrinkage and pore formation.

The X-ray diffraction patterns that characterize the phase regions of solid solutions in the La_2O_3–Er_2O_3 system at 1100 and 1500°C are shown in Figs. 7 and 8. They confirm the above results.

CONCLUSIONS

Using the data reported in [10] and our experimental results, we constructed the complete La_2O_3–Er_2O_3 phase diagram in the range 800–2400°C. This system is characterized by limited solid solutions based on various crystal modifications of the starting components and the ordered $LaErO_3$ (R) phase of perovskite type.

The ordered $LaErO_3$ (R) phase exists in the composition range 45–51 mol.% Er_2O_3 at 1100 and 1500°C. At lower temperatures, the solubility of Er_2O_3 in the hexagonal A-La_2O_3 modification decreases from 13 to 5 mol.% and the solubility of La_2O_3 in the cubic C-Er_2O_3 modification from 11 to 6 mol.%.

ACKNOWLEDGMENTS

The effort was supported by the State Fundamental Research Fund of Ukraine (Joint Ukrainian–Belarusian Project No. F73/52-2017).

REFERENCES

1. S.F. Wang, J. Zhang, D.W. Luo, F. Gu, and D.Y. Tang, “Transparent ceramics: Processing, materials and applications,” *Progr. Solid State Chem.*, **41**, 20–54 (2013).
2. J. Akiyama, Y. Sato, and T. Taira, “Laser ceramics with rare-earth-doped anisotropic materials,” *Opt. Lett.*, **35**, Issue 21, 3598–3600 (2010).
3. T. Taira, “Domain-controlled laser ceramics toward Giant Micro-photonics,” *Opt. Mater. Express,* **1**, Issue 5, 1040–1050 (2011).
4. M.A. Zelenko, S.A. Nedilko, and K.V. Degtyareva, “Conducting oxide materials based on 3*d* metals and rare earth elements,” *Fiz. Khim. Tverd. Tela*, **14**, No. 1, 108–114 (2013).
5. M. Pena and J.L.G. Fierro, “Chemical structures and performances of perovskite oxides,” *Chem. Rev.*, **101**, Issue 7, 1981–2018 (2001).

6. E.A. Magnone, “Systematic literature review on BSCF-based cathodes for solid oxide fuel cell applications,” *J. Fuel Cell Sci. Technol.*, Nos. 6–7, 1–11 (2010).
7. V.M. Goldschmidt, “The laws of crystal chemistry,” *Naturwissenschaften*, **14**, 477–485 (1926).
8. S.I. Schneider and R.S. Roth, “Phase equilibria in systems involving the rare-earth oxides. Part II: Solid state reactions in trivalent rare-earth oxide systems,” *J. Res. Nat. Bur. Stand. A: Phys. Chem.*, **64A**, No. 4, 317–332 (1960).
9. M. Foex and J.P. Traverse, “Study of polymorphism in rare earth sesquioxides at high temperatures,” *Bull. Minéral.*, **89**, No. 2, 184–205 (1966).
10. J. Coutures, A. Rouanet, R. Verges, and M. Foex, “Study of systems formed by lanthanum sesquioxides and lanthanide sesquioxides at high temperatures. I: Phase diagrams (1400°C < T < T_{liquid}),” *J. Solid State Chem.*, **17**, Nos. 1–2, 172–182 (1976).
11. S.A. Toropov, *Phase Diagrams of Refractory Oxide Systems* [in Russian], Leningrad (1987), p. 822.
12. M. Zinkevich, “Thermodynamics of rare earth sesquioxides,” *Prog. Mater. Sci.*, **52**, No. 4, 597–647 (2007).
13. Y. Zhang, *Thermodynamic Properties of Rare Earth Sesquioxides*, McGill University, Montreal, QC, Canada (2016), p. 151.
14. L.M. Lopato, A.V. Shevchenko, A.V. Kushchevskii, and S.G. Tresvyatskii, “Polymorphic transformations of rare earth oxides at high temperatures,” *Izv. AN SSSR. Neorg. Mater.*, **10**, No. 8, 1481–1487 (1974).
15. E.R. Andrievskaya, *Phase Equilibria in Systems of Hafnium, Zirconium, and Yttrium Oxides with Rare Earth Oxides: Monograph* [in Russian], Kyiv (2010), p. 470.